A Robust Controller Structure for Pico-Satellite Applications

Kragelund, Martin Nygaard; Green, Martin; Kristensen, Mads; Alminde, Lars; Bendtsen, Jan Dimon

Publication date:
2007

Document Version
Publisher's PDF, also known as Version of record

A ROBUST CONTROLLER STRUCTURE FOR PICO-SATELLITE APPLICATIONS

Martin Green [*], **Martin Kragelund** [*], **Mads Kristensen** [*], **Lars Alminde** [*], **and Jan Dimon Bendtsen** [*]

[*] *Department of Electronic Systems, Aalborg University*
{mgre02, mkr, mask02, alminde, dimon}@es.aau.dk

Abstract: This paper describes the development of a robust controller structure for use in pico-satellite missions. The structure relies on unknown disturbance estimation and use of robust control theory to implement a system that is robust to both unmodeled disturbances and parameter uncertainties. As one possible application, a satellite mission with the purpose of monitoring shipping routes for oil spills has been considered. However, it is the aim of the control structure to be widely applicable and adaptable for a wide variety of pico-satellite missions. The robust control structure has been evaluated using Monte Carlo simulations.

Keywords: Attitude control, robust control, disturbance estimation.

1. INTRODUCTION

In recent years Aalborg University has been active in developing pico-satellites, i.e., satellites of $1-10$ [kg]. In 2003, AAU-Cubesat was among the first CubeSats to be launched [Alminde et al., 2004], and in the summer of 2007 another CubeSat, AAUSAT-II, will be launched featuring an advanced attitude control system with reaction wheels [AAUSAT-II].

This paper deals with a prestudy of a possible third satellite in the series, called the North Sea Observer (NSO) - A triple CubeSat weighing 3 [kg] and dimensions of $30\,[\text{cm}] \times 10\,[\text{cm}] \times 10\,[\text{cm}]$. The primary objective of the NSO will be to monitor shipping routes in the North Sea using a high resolution digital camera, and search for oil spills from seagoing vessels in these waters. Due to mandatory Automatic Identification System (AIS) transponder technology on board ships, it will be possible to correlate oil spill findings with the trajectory of ships to identify the culprit. The satellite is foreseen to be launched into a circular solar synchronous orbit, with an altitude between 400 [km] and 800 [km].

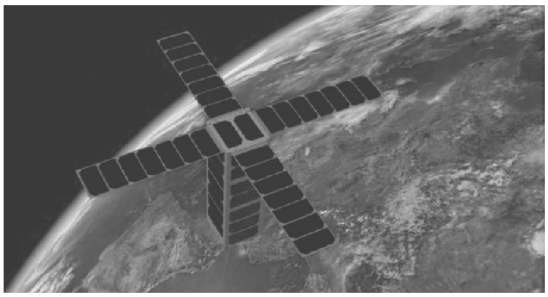

Figure 1. The North Sea Observer in orbit.

The NSO will reuse some of the existing subsystem technologies developed for AAUSAT-II, but will feature a new deployable solar array on each lateral side panel, in order to increase power production. An artist's impression of the NSO in orbit can be seen in Figure 1. The NSO is currently in the feasibility phase (A) of the ECSS standard classification [ESTEC, April 1996].

The satellite will rely on a high-precision, low economical cost Attitude Determination and Control System (ADCS), to limit the rotational velocity of the satellite and enable pointing of the on-board camera towards a location in the North Sea.

1.1 NSO Attitude Control System

After separation from the launch vehicle the NSO will deploy the solar panels. An inertia matrix for the satellite in this situation has been calculated based on the following assumptions:

- The solar arrays have the dimension 30 [cm]$\times$ 10 [cm] $\times$ 0.2 [cm].
- The combined mass of the solar arrays is 0.5 [kg], i.e., 0.125 [kg] each.
- The satellite body has no loss in dimensions, when the solar arrays have been deployed.
- The complete satellite structure is considered a single rigid body.

This leads to the following inertia matrix around the combined center of mass

$$\mathbf{I}_{\text{sat}} = \begin{bmatrix} 0.0423 & 0 & 0 \\ 0 & 0.0423 & 0 \\ 0 & 0 & 0.0283 \end{bmatrix} \quad [\text{kgm}^2]. \quad (1)$$

The attitude control system is a scaled-up version of the AAUSAT-II system. The satellite is equipped with the following actuators:

Momentum wheels: Three momentum wheels are mounted orthogonally in the satellite, capable of producing an angular momentum of $\pm \begin{bmatrix} 2.23 & 2.23 & 2.23 \end{bmatrix}^T \cdot 10^{-3}$ [kgm^2/s].

Magnetorquers: Three coils are implemented as an embedded part of three orthogonally side panels and are used for momentum unloading. The maximum magnetic moment of the coils is $\begin{bmatrix} 202.97 & 202.97 & 135.31 \end{bmatrix}^T \cdot 10^{-3}$ [Am^2].

Adopting the sampling capabilities from the avionics of AAUSAT-II, it is possible to utilise a maximum sampling frequency of $1 \cdot 10^3$ [Hz].

1.2 Paper Outline

A complete control system has been developed including:

{1} Robust angular velocity controller based on momentum wheels.
{2} Disturbance feedforward based on estimation of unknown torques.
{3} Pointing controller that provides reference to the angular controller.
{4} Desaturation controller that executes in parallel using magnetorquers.

This paper will focus on {1} and {2}. The performance of the on-board Attitude Determination System (ADS) is not considered at this point in the development, and hence knowledge of the attitude is assumed perfect in this paper. Future work will include the effects of ADS estimation errors on the combined performance.

The following section will describe the structure of the controller, whereafter Section 3 will describe the feed-forward compensation of unknown disturbances. Hereafter, the development of the robust angular controller will be described and the complete system will be evaluated upon which final conclusions will be drawn.

All simulations have been performed using a modified version of the in-house developed high-fidelity simulation environment for MATLAB/SIMULINK presented in [Amini et al., 2005].

In this paper all matrices and vectors are typed with boldface, e.g., the identity matrix is written as $\mathbf{1}$.

2. CONTROLLER STRUCTURE

After deployment, the solar panels of the NSO present a challenge due to the time varying density of the residual atmosphere, which makes it difficult to estimate the disturbance torques induced a-priori. In addition, the accelerated development schedule and reduced budget pursued in the pico-satellite program, entails that on-ground calibration/estimation of parameters, such as exact moments and products of inertia, is often not possible. [Peck, 2003]

The above suggests designing a robust controller that can handle both input disturbances, i.e., external disturbance torques, and parametric uncertainties due to the imperfect system knowledge. However, as the disturbance torques can be large, this approach is likely to yield a slow response of the closed loop system, since the controller is not allowed to be aggressively tuned. To avoid this, and decouple the effects of the external disturbance torques, the angular velocity controller is divided into a disturbance estimator and a robust controller. The described control structure is depicted in Figure 2.

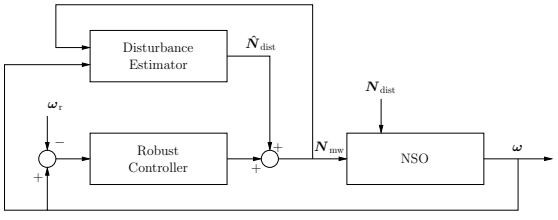

Figure 2. Block diagram of controller structure.

The estimated total disturbance torque is fed forward to attenuate the input disturbance to the satellite. This accounts for both uncertainties in modeled disturbances and effects of disturbances that are not modeled, as will be shown in the following section.

The only parametric uncertainty that will be considered for the robust angular velocity controller will be variations in the diagonal components of the inertia matrix (1).

3. DISTURBANCE ESTIMATION

The nominal pointing of NSO is towards Nadir, with some limited off-pointing when tracking targets. Therefore, from a satellite perspective the environmental disturbance torques will vary slowly and can be modeled as a constant bias in the control torque. This yields an estimation of the disturbance torque, which is independent of the disturbance models. Thus, the model parameters, such as the highly uncertain air density will not affect the estimation and no on-board disturbance models are required. The system considered in the disturbance estimation is defined as

$$\begin{bmatrix} \dot{\boldsymbol{\omega}} \\ \dot{\boldsymbol{N}}_{\text{dist}} \end{bmatrix} = \begin{bmatrix} \mathbf{I}_{\text{sat}}^{-1}\mathbf{S}(\bar{\boldsymbol{h}}_{\text{mw}}) & \mathbf{I}_{\text{sat}}^{-1} \\ \mathbf{0}_{3\times 3} & \mathbf{0}_{3\times 3} \end{bmatrix} \begin{bmatrix} \boldsymbol{\omega} \\ \boldsymbol{N}_{\text{dist}} \end{bmatrix} + \begin{bmatrix} -\mathbf{I}_{\text{sat}}^{-1} \\ \mathbf{0}_{3\times 3} \end{bmatrix} \boldsymbol{N}_{\text{mw}}, \quad (2)$$

where $\boldsymbol{\omega}$ is the angular velocity vector of the satellite and $\boldsymbol{N}_{\text{dist}}$ and $\boldsymbol{N}_{\text{mw}}$ are the disturbance torque and the control torque from the momentum wheels respectively. $\mathbf{S}(\bar{\boldsymbol{h}}_{\text{mw}})$ denotes the skew symmetric matrix containing the angular momentum bias vector. The estimated total disturbance torque is fed forward to the momentum wheel control input to attenuate the input disturbance.

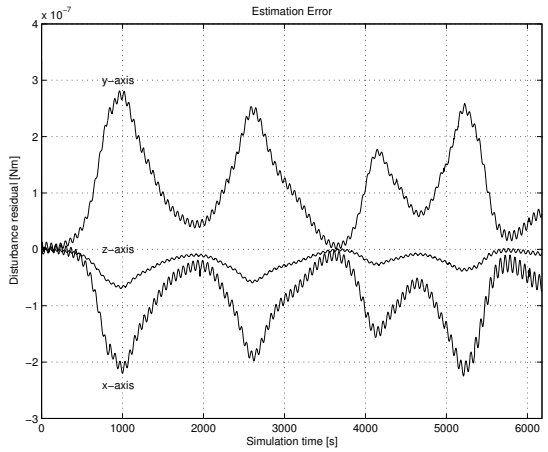

Figure 3. The estimation error between the modeled disturbance torque and the estimated torque.

It is chosen to implement the disturbance estimation in a Kalman filter using the system in (2). The Kalman gain is calculated using the noise description of the measurement and the process, $\mathbf{R}_{\text{ang}}$ and $\mathbf{Q}_{\text{ang}}$ respectively. The noise descriptions are determined empirically from simulation models, as $\mathbf{R}_{\text{ang}} = 10^{-12} \cdot \mathbf{1}_{3\times 3}$, and $\mathbf{Q}_{\text{ang}} = 5 \cdot 10^{-15} \cdot \mathbf{1}_{6\times 6}$ are defined, such that the system model is trusted more than the measurement, thus allowing a slow change in the state estimates.

A Monte Carlo evaluation of the filter indicates that the mean estimation error is $31.2 \cdot 10^{-9}$ [Nm] and the standard deviation is $50.2 \cdot 10^{-9}$ [Nm], which corresponds to 2 [%] of the worst case disturbance torque, thus providing that the desired effect of the Kalman filter is achieved. The estimation error of a simulation using the worst case air density is depicted in Figure 3.

4. ROBUST ANGULAR VELOCITY CONTROL

The estimation of the disturbance torques yields a small residual error as described in the previous section. Therefore, the angular controller should be able to handle the remaining input disturbance. Furthermore, it is difficult to achieve precise knowledge of all the parameters in the model, which the controller should also account for.

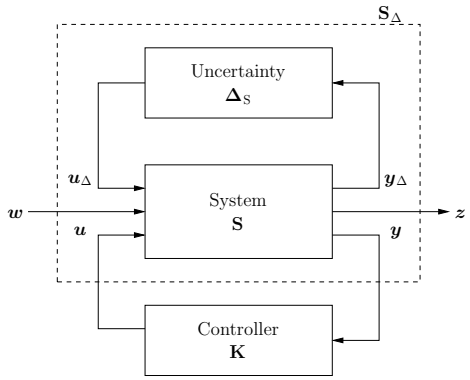

Figure 4. General control structure for cases with model uncertainties [Skogestad and Postlethwaite, 2005, page 113].

In Figure 4 the uncertainties are lumped into one uncertainty system, $\boldsymbol{\Delta}_{\text{S}}$, with $\boldsymbol{y}_{\Delta}$ and $\boldsymbol{u}_{\Delta}$ as input and output respectively. The perturbed system, $\mathbf{S}_{\Delta}$, is controlled by $\mathbf{K}$, with the control signal $\boldsymbol{u}$ and the sensed output $\boldsymbol{y}$. The objective of robust control is to find a controller, $\mathbf{K}$, that minimises a norm of the transfer function from external input, $\boldsymbol{w}$, to the performance output, $\boldsymbol{z}$ [Skogestad and Postlethwaite, 2005]. For instance, $\mathcal{H}_{\infty}$ controller synthesis refers to solving the optimisation problem

$$\min_K \|\mathbf{F}_l(\mathbf{S},\mathbf{K})\|_\infty. \tag{3}$$

where $\mathbf{F}_l(\mathbf{S},\mathbf{K})$ denotes the lower Linear Fractional Transformation (LFT) of $\mathbf{S}$, with $\mathbf{K}$ being a parameter.

Several methods for solving this problem exist and in this paper an LMI based solution will be used for describing the uncertainty system.

4.1 LMI Formulation for Robust Feedback Control

To formulate the requirement of robustness to uncertainties, but also the requirement to suppress the effects of input disturbances, the focus is turned to the work done in [Zhou et al., 1995], where linear time-invariant systems with real time-varying parameter uncertainties in compact intervals are considered. The main results they presented, showed that both analysis and state feedback synthesis problems, can be reduced to a finite-dimensional convex programming problem. From [Zhou et al., 1995] we have the following results:

Theorem 1: Consider the uncertain system

$$\begin{aligned}
\dot{\boldsymbol{x}} &= \mathbf{A}_\Delta \boldsymbol{x} + \mathbf{B}_\Delta \boldsymbol{w} + \mathbf{B}_{2\Delta}\boldsymbol{u}, \quad \Delta \in \underline{\boldsymbol{\Delta}} \\
\boldsymbol{z} &= \mathbf{C}_\Delta \boldsymbol{x} + \mathbf{D}_\Delta \boldsymbol{w} + \mathbf{D}_{2\Delta}\boldsymbol{u} \\
\boldsymbol{y} &= \boldsymbol{x},
\end{aligned} \tag{4}$$

and suppose that there exists a dynamic state feedback controller $\boldsymbol{u} = \mathbf{F}(s)\boldsymbol{y}$, such that the closed-loop system satisfies the strongly robust $\mathcal{H}_\infty$ performance criterion. Then there exists a real matrix $\mathbf{K}$, such that, with the static controller $\boldsymbol{u} = \mathbf{K}\boldsymbol{y}$, the closed-loop system satisfies the strongly robust $\mathcal{H}_\infty$ performance criterion.

Theorem 2: There exists a state feedback controller, such that the above closed-loop system satisfies the strongly robust $\mathcal{H}_\infty$ performance criterion if and only if $\mathbf{R}_\Delta \triangleq \mathbf{1} - \mathbf{D}_\Delta^T\mathbf{D}_\Delta \succ 0$, $\forall \Delta \in \underline{\boldsymbol{\Delta}}_{\text{vex}}$ and there exists a matrix $\mathbf{W}$ and a matrix $\mathbf{Y} = \mathbf{Y}^T \succ 0$, such that

$$0 \succ \begin{bmatrix} \mathbf{Y}\mathbf{A}_\Delta^T + \mathbf{A}_\Delta\mathbf{Y} + \mathbf{W}^T\mathbf{B}_{2\Delta}^T + \mathbf{B}_{2\Delta}\mathbf{W} & \Phi & \Psi \\ \Phi^T & -\mathbf{R}_\Delta & \mathbf{0} \\ \Psi^T & \mathbf{0} & -\mathbf{1} \end{bmatrix}$$

$$\forall \quad \Delta \in \underline{\boldsymbol{\Delta}}_{\text{vex}}\,, \tag{5}$$

where

$$\begin{aligned}
\Phi &= \mathbf{B}_\Delta + \mathbf{Y}\mathbf{C}_\Delta^T\mathbf{D}_\Delta + \mathbf{W}^T\mathbf{D}_{2\Delta}^T\mathbf{D}_\Delta \\
\Psi &= \mathbf{Y}\mathbf{C}_\Delta^T + \mathbf{W}^T\mathbf{D}_{2\Delta}^T\,.
\end{aligned}$$

Moreover, the scalar feedback controller can be taken as a constant gain as

$$\mathbf{K} = \mathbf{W}\mathbf{Y}^{-1}\,. \tag{6}$$

The condition $\mathbf{R}_\Delta \succ 0$ ensures that the direct feed-through of the disturbances is less than one, i.e., $\|\mathbf{D}_\Delta\| < 1$.

Hence, if it is possible to find a $\mathbf{K}$ satisfying the requirements in *Theorem 2* for the uncertain disturbed angular velocity system, the closed loop will be stable and achieves strongly robust performance. However, due to hardware limitations, the closed loop must also meet certain bandwidth restrictions, as mentioned in Section 1. This can be ensured by restraining the real part of the closed loop left half plane poles to be no less than a certain limit, η. This is achieved by including another constraint in the LMI in (5).

According to [Chilali and Gahinet, 1996, eq. (18)] bounding eigenvalues in a matrix $\mathbf{A}$ to lie above a specified lower limit, can be expressed in an LMI as

$$2\eta\mathbf{P} - \mathbf{A}^T\mathbf{P} - \mathbf{P}\mathbf{A} \prec 0, \tag{7}$$

where η is the positive boundary distance from the imaginary axis along the negative real axis, if and only if there exists a symmetric matrix $\mathbf{P} \succ 0 \in \mathbb{R}^{n\times n}$. It is desired, instead of bounding the eigenvalues in the matrix $\mathbf{A}$, to bound the poles in the closed loop system, whereby the matrix $\mathbf{A}$ is substituted with the dynamics of the closed loop, i.e., $\mathbf{A} = \mathbf{A}_\Delta + \mathbf{B}_{2\Delta}\mathbf{K}$. Using $\mathbf{Y} \triangleq \mathbf{P}^{-1}$ and defining $\mathbf{W} = \mathbf{K}\mathbf{Y}$, yields

$$2\eta\mathbf{Y} - \mathbf{Y}\mathbf{A}_\Delta^T - \mathbf{W}^T\mathbf{B}_{2\Delta}^T - \mathbf{A}_\Delta\mathbf{Y} - \mathbf{B}_{2\Delta}\mathbf{W} \prec 0. \tag{8}$$

Thus an LMI feasibility problem [1] has been obtained in the new variables $\mathbf{Y} \succ 0$ and $\mathbf{W} \in \mathbb{R}^{m\times n}$. This can now be augmented to the LMI in (5), yielding an LMI formulation ensuring both strongly robust $\mathcal{H}_\infty$ performance and a bounded bandwidth by restricting the variables in (5). Since $\mathbf{Y} \succ 0$ and $\mathbf{Y}^T = \mathbf{Y}$ the feedback matrix, $\mathbf{K}$, can now be recovered analogously to (6) by

$$\mathbf{W} = \mathbf{K}\mathbf{Y} \Rightarrow \mathbf{K} = \mathbf{W}\mathbf{Y}^{-1}. \tag{9}$$

Bounding the poles to lie to the left of the imaginary axis is still handled by the LMI in (5).

An LMI feasibility problem, ensuring the bandwidth bounded closed loop stability and performance of an uncertain disturbed system, has now been formulated.

4.2 Angular Controller Design

As stated earlier the disturbance, considered in this paper, is the environmental disturbance torque residual, which enters the system in a similar manner as the control torques, i.e., the only difference is a change of sign

$$\mathbf{B}_{\text{dist}} = -\mathbf{B}_{\text{ctrl}}\,. \tag{10}$$

[1] Problems for which a solution is sought, which might not be unique or optimal.

The uncertainty considered is imprecise knowledge of the values in the diagonal of the inertia matrix, which is estimated to vary $\pm 5\,[\%]$, i.e.,

$$\mathbf{I}_\Delta = \mathbf{I}_{\text{sat}} \pm 0.05 \cdot \mathbf{I}_{\text{sat}}\,. \tag{11}$$

The objective of the controller is to minimise the angular velocity of the satellite, such that it is possible to obtain pictures of the North Sea. As the camera is located on the z-axis, rotation around this axis is not as critical as around the x and y-axes. Therefore, the external output, $\boldsymbol{z}$, is chosen to be ω_{x} and ω_{y}, yielding the uncertain system

$$\begin{aligned}\dot{\boldsymbol{\omega}} &= \underbrace{\mathbf{I}_\Delta \mathbf{S}(\bar{\boldsymbol{h}}_{\text{mw}})}_{\mathbf{A}_\Delta}\boldsymbol{\omega} + \underbrace{\mathbf{I}_\Delta}_{\mathbf{B}_\Delta}\boldsymbol{N}_{\text{dist}} \underbrace{-\mathbf{I}_\Delta}_{\mathbf{B}_{2\Delta}}\boldsymbol{N}_{\text{mw}} \\ \boldsymbol{z} &= \underbrace{\begin{bmatrix}\mathbf{1}_{2\times 2} & \mathbf{0}_{2\times 1}\end{bmatrix}}_{\mathbf{C}_\Delta}\boldsymbol{\omega} + \underbrace{\mathbf{0}_{2\times 3}}_{\mathbf{D}_\Delta}\boldsymbol{N}_{\text{dist}} + \underbrace{\mathbf{0}_{2\times 3}}_{\mathbf{D}_{2\Delta}}\boldsymbol{N}_{\text{mw}},\end{aligned} \tag{12}$$

which is exactly on the form presented in (4).

The YALMIP toolbox is used to formulate the LMI presented in the previous section, for all of the vertices in the uncertainty region. The problem is then solved using SeDuMi. As the inertia matrix contains three parameters, the uncertainty region will become a cube.

The LMI derived assumes the objective is to obtain a $\mathcal{H}_\infty$ norm less than one, but it is desirable to define a value, γ, such that the $\mathcal{H}_\infty$ norm is less than γ, and then iterate to obtain the smallest possible $\mathcal{H}_\infty$ norm, yielding a near optimal solution of the LMI feasibility problem. This is incorporated by considering $\|\mathbf{F}_l(\mathbf{S},\mathbf{K})\|_\infty$, which yields

$$\gamma > \|\mathbf{F}_l(\mathbf{S},\mathbf{K})\|_\infty \Rightarrow 1 > \left\|\frac{1}{\gamma}\mathbf{F}_l(\mathbf{S},\mathbf{K})\right\|_\infty\,. \tag{13}$$

Combining this with the system defined in (12), yields a scaling of $\mathbf{B}_\Delta$ with $\frac{1}{\gamma}$. From an iterative process it is found that $\gamma = 20\,[.]$, yields feasibility of the LMI.

Considering the dynamics and kinematics of the satellite, the bandwidth of the angular velocity controller should be $0.2\,[\text{Hz}]$ or less, i.e., the real values of the closed loop poles should reside between $-0.2\cdot 2\pi\,[\text{rad/s}]$ and $0\,[\text{rad/s}]$. The boundary in the pole-limiting LMI is therefore chosen to be $\eta = 0.2 \cdot 2\pi\,[\text{rad/s}]$, as η is defined positively in the LMI.

The combined LMI is implemented and solved using MATLAB and yields a state feedback controller defined as

$$\mathbf{K}_{\text{ang}} = \begin{bmatrix} 0.0506 & -0.0001 & -0.0003 \\ -0.0001 & 0.0506 & -0.0003 \\ -0.0003 & -0.0001 & 0.0340 \end{bmatrix}. \tag{14}$$

Closing the loop with this state feedback controller, yields the poles depicted in Figure 5, where it is noticed that the poles are all above the limit of $-0.2 \cdot 2\pi \approx -1.256\,[\text{rad/s}]$. The Δ marks the poles of the nominal system, and the $\times$ marks the poles of the closed loop system at each of the vertices of the uncertainty region.

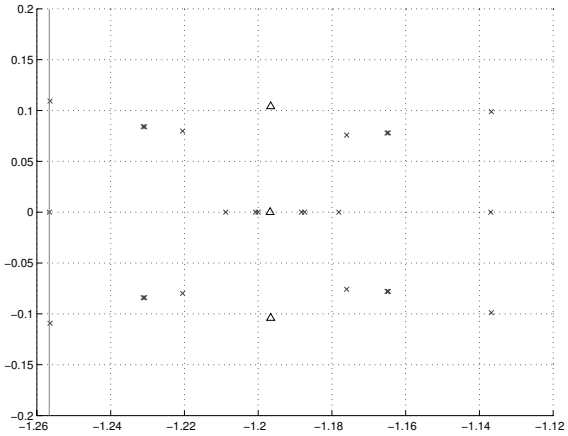

Figure 5. Pole locations with robust controller.

The angular velocity controller, including the disturbance estimator, has been implemented in SIMULINK.

5. PERFORMANCE EVALUATION

A Monte Carlo simulation approach has been adopted, to evaluate the designed robust angular velocity controller. In order to reduce simulation time the Monte Carlo approach is limited to the nominal inertia matrix and the 8 corner matrices in the uncertainty region. For each inertia matrix the drag coefficient, air density and initial attitude quaternion are randomly chosen, and the system is simulated 30 times to obtain a valid statistical result. Since the three parameters are uncorrelated, they are changed simultaneously under the constraints described below.

- The drag coefficient, C_{D}, is chosen randomly in the interval $[1; 2]\,[.]$.
- The air density, ρ_{air}, is chosen randomly in the interval $[4 \cdot 10^{-14}; 7.23 \cdot 10^{-12}]\,[\text{kg/m}^3]$.
- The initial attitude quaternion is chosen randomly, complying with the constraint $\|\boldsymbol{q}\| = 1$.

This yields a total of 270 simulations. Figure 6 depicts the angular velocity during an entire orbit, where the angular velocity settles at approximately zero within $14\,[\text{s}]$ from an initial velocity, $\boldsymbol{\omega}_{\text{init}} = [0.0021 \;\; -0.0021 \;\; 0.0021]\,[\text{rad/s}]$. The angular velocity controller without estimation and feedforward is capable of attenuating the disturbance torques.

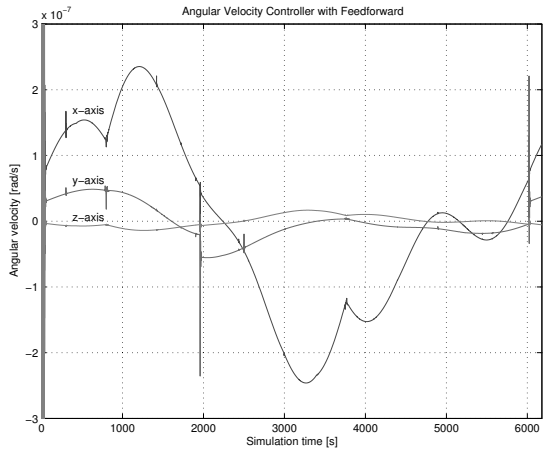

Figure 6. Angular velocity from a simulation of a complete orbit using disturbance estimation and feedforward. The small spikes arise from switching between disturbance models and the two larger spikes arise from eclipse transitions.

However, the introduction of the estimation and feedforward improves the controller's ability to attenuate the disturbance torques with a factor of six, such that the mean angular velocity of the satellite is

$$\boldsymbol{\mu}_\omega = [600 \;\; 95 \;\; -14.7] \cdot 10^{-12}\,[\text{rad/s}]. \qquad (15)$$

To give an indication of the newfound robust controller's ability to cope with uncertainties and disturbances, it is compared to a simple, but fully tuned pole placed state feedback controller using an analogous Monte Carlo approach, where the two controller types are submitted to identical parameter fluctuations.

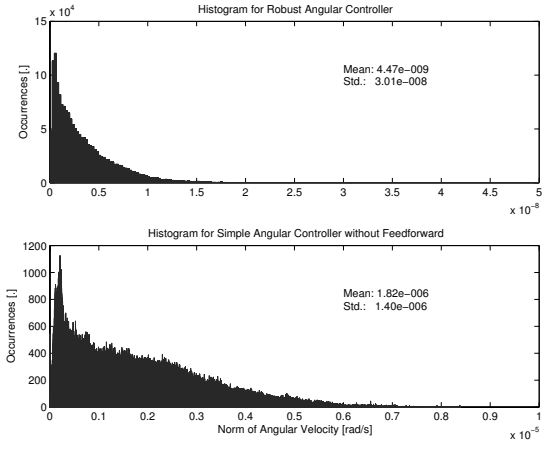

Figure 7. Distribution of the angular velocity norm for both the robustly controlled system and the pole placed state feedback controlled system. Note the different x-axis scale in the two histograms.

Figure 7 depicts the statistical outcome of the comparison of the length of the angular velocity vector, where it is certainly worth noticing the difference in the x-axis scale. Referring to Figure 7 for further details, it is easily noticeable that the designed robust controller is statistically far better at suppressing the angular velocity than the simple counterpart.

Furthermore, the angular velocity controller is capable of following a reference signal and is, therefore, considered appropriate for attitude control.

6. CONCLUSIONS AND PERSPECTIVES

This paper has presented a control structure that features estimation of unknown disturbances and a robust feedback controller in order to provide a robust system for control of pico-satellites equipped with momentum wheels. This can be used when on-ground calibration/estimation of parameters such as exact moments of inertia is not possible. The designed control structure improved the mean angular velocity by approximately 400 times compared to a pole placed state feedback controller. Furthermore, the robust controller is a simple constant feedback matrix, which does not entail more computational demands than the pole placed state feedback controller.

Further work will evaluate performance with a proper attitude determination system, which includes some estimation noise. Introducing the ADS facilitates for inclusion of the disturbance estimation in this system, thus reusing the models utilised. The uncertainties considered in this paper could be extended to include models of, e.g., misalignment of the actuators.

REFERENCES

AAUSAT-II. URL `http://www.aausatii.aau.dk`.

Lars Alminde, Morten Bisgaard, Dennis Vinther, Tor Viscor, and Kasper Østergaard. *AAU-Cubesat Architectual Overview and Lessons Learned.* IFAC, 2004. Proceedings of the 16th IFAC Symposium on Automatic Control in Aerospace, 2004, Sct. Petersburg, Russia.

Rouzbeh Amini, Jesper A. Larsen, Roozbeh Izadi-Zamanabadi, and Dan D. V. Bhanderi. Design and implementation of a space environment simulation toolbox for small satellites. In *In Proc.: 25th International Astronautical Congress*, October 2005.

Mahmoud Chilali and Pascal Gahinet. h_∞ design with pole placement constraints: An lmi approach. *Automatic Control*, 41(3):358–367, March 1996.

Requirements & Standards Division ESA ESTEC. *Space Project Management - Project Phasing and Planning.* April 1996.

Mason A. Peck. *Uncertainty Models for Physically Realizable Inertia Dyadics.* 2003. Presented at the 2003 Flight Mechanics Symposium, Goddard Space Flight Center, Greenbelt, MD.

Sigurd Skogestad and Ian Postlethwaite. *Multivariable Feedback Control - Analysis and Design.* John Wiley and Sons Ltd, 2005. ISBN 978-0-470-01168-3.

Kemin Zhou, Pramod P. Khargonekar, Jacob Stoustrup, and Hans Henrik Niemann. Robust performance of systems with structured uncertaities in state space. *Automatica, Vol. 31, No.2*, 1995.